MAGNETORHEOLOGICAL LANDING GEAR.

PART 1: A DESIGN METHODOLOGY

D C Batterbee[†], N D Sims[†*], R Stanway[†], and Zbigniew Wolejsza[‡]

[†]Department of Mechanical Engineering, The University of Sheffield,
Sheffield, S1 3JD, UK.

[‡]The Institute of Aviation, Al. Krakowska 110/114, 02-256 Warsaw, Poland.

ABSTRACT

Aircraft landing gears are subjected to a wide range of excitation conditions, which result in conflicting damping requirements. A novel solution to this problem is to implement semi-active damping using magnetorheological (MR) fluids. This paper presents a design methodology that enables an MR landing gear to be optimised, both in terms of its damping and magnetic circuit performance, whilst adhering to stringent packaging constraints. Such constraints are vital in landing gear, if MR technology is to be considered as feasible in commercial applications.

The design approach focuses on the impact or landing phase of an aircraft's flight, where large variations in sink speed, angle of attack and aircraft mass makes an MR device potentially very attractive. In this study, an equivalent MR model of an existing aircraft landing gear is developed. This includes a dynamic model of an MR shock strut, which accounts for the effects of fluid compressibility. This is important in impulsive loading applications such as landing gear, as fluid compression will reduce device controllability. Using the model, numerical impact simulations are performed to illustrate the performance of the optimised MR shock strut, and hence the effectiveness of the proposed design methodology. Part 2 of this contribution focuses on experimental validation.

KEYWORDS: Magnetorheological, aircraft landing gear, semi-active damping, smart fluids, impacts

[*] Corresponding author. Email: n.sims@sheffield.ac.uk; Tel: +44 (0)114 2227724.

NOTATION

a_{2i}	Piston area
a_{2o}	Outer cross-sectional area of inner cylinder
b	Mean annular circumference of valve
B_f	Magnetic flux density in the fluid
B_s	Magnetic flux density in the steel
c	Tyre constant
d	Mean valve diameter
D	Piston diameter
F_s	Shock strut force
F_t	Tyre force
g	Acceleration due to gravity ($9.81 ms^{-2}$)
h	Valve gap height
h_c	Coil height
H_f	Magnetic field strength in the fluid
H_s	Magnetic field strength in the valve material
I	Current
l	Constrained length of valve
l_a	Active valve length
l_t	Total length of multi-staged valve
L	Lift
m	Gas exponent
m_p	Mass of aircraft or drop mass
m_w	Mass of wheel and tyre assembly
n	Stage number
p	Power
P	Pressure
P_1	Fluid pressure in chamber 1
P_2	Fluid pressure in chamber 1
P_a	Gas pressure
P_{a0}	Initial gas pressure
Q	Volume flow rate
Q_{max}	Maximum valve flow rate during impact
r	Tyre exponent
R_c	Resistance of coil
Re	Reynolds number
Re_c	Critical Reynolds number
t	Time
t_a	Bobbin core radius
t_b	Bobbin flange height
t_d	Deflection time
v	Fluid volume
v_{10}	Initial fluid volume in chamber 1
v_{20}	Initial fluid volume in chamber 2
v_a	Gas volume
v_{a0}	Initial gas volume
V_{sink}	Aircraft sink velocity
w_c	Coil width
z	Displacement of SDOF impact system
z_p	Displacement of aircraft or drop mass
z_w	Displacement of wheel and tyre assembly
$\ddot{z}_{t_d}$	Critical acceleration to cause shock strut deflection
α	Dimensionless valve length
β	Bulk modulus of the fluid
ΔP_{l_a}	Pressure drop across the active valve length
ΔP_0	Zero field valve pressure drop
ΔP_{max}	Maximum valve pressure drop (Active + inactive)
ΔQ	Net volume flow rate
λ	Control ratio
μ	Viscosity of MR fluid
ρ	Density of MR fluid
τ	Time constant
τ_y	MR fluid yield stress
$\tau_{y_{max}}$	Maximum MR fluid yield stress

1 INTRODUCTION

Aircraft landing gears are subjected to a wide range of impact conditions due to variations in sink speed, angle of attack and mass. The landing gear must be able to absorb sufficient energy in severe impacts or crash landing scenarios in order to minimise structural damage. To accommodate this requirement, the performance for more common (i.e. less severe) impacts will be compromised, and this may reduce the structure's fatigue life and increase levels of passenger discomfort. Conflicting damping requirements between the landing impact and taxiing phases results in further performance compromises [1]. In the 1970's, NASA researchers began the development of active landing gear concepts in order to overcome these passive limitations [2]. However, such technologies have not come to fruition as a result of their large size, weight and power requirements. A more attractive solution is to implement semi-active energy dissipation using smart fluids. Such fluids allow the continuous adjustment of damping force through the application of either an electric field (for electrorheological (ER) fluids) or a magnetic field (for magnetorheological (MR) fluids). For both fluids, polarisation causes the formation of particle chains and hence the development of a controllable yield stress within the smart device. In comparison to active devices, smart dampers are less complex, have lower power requirements, and can be better packaged within a limited space.

Practical ER fluids were produced over two decades ago [3]. However, their use in the aerospace industry was ruled out, owing to a reluctance to provide the voltages required to generate electric fields of up to 4kV/mm [4]. In addition, ER fluids have a narrow working temperature range [5], making them unsuitable for high altitudes. Consequently, the application of smart fluids in the aerospace industry, and more specifically in aircraft landing

gears, was until recently, largely unexplored. The more recent developments in MR fluids have led to a renewed interest in this field. In contrast to ER fluids, MR fluids are powered by a low voltage source and have been shown to be capable of operating between -40°C and 150°C [6]. Consequently they are far better suited to aerospace applications, and will therefore be the focus of the present study.

The use of smart fluids in landing gear has been considered previously, and various configurations of device have been considered [7-9]. Lou *et al.* [7] presented a shear mode ER landing gear, which used a device to convert translational motion of the piston rod into rotational motion between shearing disks. Berg and Wellstead [8] developed a shear/squeeze mode ER device, which was numerically investigated in series with a conventional passive landing gear. Finally, Choi and Wereley [9] investigated the use of a flow mode ER/MR landing gear shock strut, and concluded that accelerations can be significantly attenuated using a sliding mode controller.

Whilst these earlier investigations have helped to demonstrate the benefits of using smart fluids in landing gear, they have often overlooked packaging requirements/constraints and the effects of fluid compressibility in numerical models. Adhering to sizing constraints is vital if the feasibility of a new landing gear concept is to be proven. Furthermore, the consideration of fluid compressibility is particularly important in impulsive loading applications, as fluid compression will reduce valve flow and hence controllability. Consequently, the aim of the present research is to investigate the feasibility of an MR landing gear through direct consideration of the packaging constraints. This will involve the use of a dynamic landing gear model that accounts for fluid compressibility thus enabling an accurate prediction of performance. The study focuses on the impact phase of an aircraft's landing, where the loads

are at their largest and most unpredictable levels, and the effect on the fatigue life of structural components is most significant.

Part 1 of this contribution is organised as follows. A numerical design approach is first presented, which extends upon previous work by the authors [10]. The approach enables dynamic impact performance predictions, and MR device optimisation within the sizing constraints of existing landing gears. A case study is then presented to demonstrate the proposed design methodology. This uses data from a commercial (passive) landing gear, which serves as a performance benchmark and provides the necessary sizing constraints for the MR design. Experimental validation of the numerical design methodology is the focus of Part 2, and the combined contribution should make a significant step towards demonstrating the feasibility of MR landing gears.

2 THE DESIGN METHODOLOGY

The most common configuration of shock absorber found on aircraft is oleopneumatic, which combine oil and gas for damping and stiffness purposes respectively. This is due to their relatively high impact efficiencies and low weight [11]. An example of an oleopneumatic shock absorber (often referred to as the shock strut) is shown in Figure 1(a). Here, as the shock strut compresses, fluid is forced turbulently through the main orifice in the piston head, giving rise to a damping effect. The fluid subsequently compresses the gas in the upper chamber, providing a non-linear stiffness effect. As shown, metering pins are sometimes used to improve impact efficiency by regulating the orifice size as a function of piston displacement.

The MR landing gear design methodology is based upon replacing the passive orifice shown in Figure 1 with an MR valve. This dictates the packaging constraints of the MR device. The

aim is then to find a way of designing the valve such that the landing gear can achieve an optimal performance over a range of impact scenarios. This optimisation must include an analysis of the magnetic circuit design.

The MR valve configuration investigated in this study is shown in Figure 2. Here, fluid flows through an annular orifice and the magnetic flux is generated via a coil wrapped around a steel bobbin. The active section of the valve (i.e. the length exposed to the magnetic field) is observed where the path of magnetic flux crosses the annular orifice. The fluid volume adjacent to the coil remains inactive.

It transpires that the geometry of this device can be optimised from a magnetic perspective using analytical methods, and is relatively insensitive to the valve gap *h*. In contrast the damping behaviour is difficult to optimise because of the nonlinear interaction between fluid flow, tyre deflection, and shock strut gas compression. It is, however, highly sensitive to the valve gap *h*.

The landing gear design approach that was developed is summarised in Figure 3. To begin, the MR shock absorber is sized to be that of the equivalent passive device, in terms of its length and diameter. This constrains the values for the external geometry of the MR valve (length *l* and diameter *D*). Initial estimates for the valve's flow diameter *d* and active length l_a can then be determined. At this stage the precise values are not important because they will be optimised later, from a magnetic standpoint.

Landing impact simulations are then performed, using data for the actual aircraft structure, to predict behaviour. This is performed for the case where the fluid yield stress is at its maximum value $\tau_{y_{\max}}$, and the impact scenario is at its most severe. Consequently, for less severe impacts with lower damping requirements, the yield stress can be controlled to give

superior performance over the existing passive system. In this worst-case configuration, the valve gap h is modified to achieve desirable landing behaviour, for example by comparison with the behaviour of a passive device. From this result, the pressure drop ΔP_{max} at maximum valve flow rate Q_{max} is determined, and the two properties ΔP_{max}, Q_{max}, are used to characterise the requirement of the valve.

The task now is to optimise the magnetic performance of the valve, whilst still achieving the desirable (ΔP_{max}, Q_{max}) characteristic. Furthermore, the aim is to maximise the controllability of the valve, thus maximising the range of impact conditions that can be accommodated. This involves revising the valve's mean radius and active length, choosing the electric circuit configuration, and finally modifying the valve gap so as to maintain the (ΔP_{max}, Q_{max}) characteristic. Because the magnetic behaviour is relatively insensitive to the valve gap, it is not normally necessary to repeat the magnetic optimisation once the valve gap h has been finally chosen.

Once the final valve geometry has been chosen, the landing impact simulations can be repeated to check that the performance is close to that found for the preliminary design. Because the (ΔP_{max}, Q_{max}) characteristic is largely unchanged, the damping performance will not differ greatly between the magnetically optimised design and the preliminary design.

The design methodology requires two modelling approaches: a time-domain landing simulation including MR damping, and an analytical approach for optimising the magnetic design of the valve.

3 THEORY

So far, a design methodology has been presented that aims to enhance the impact performance of MR landing gears subjected to packaging constraints. The methodology uses various numerical tools, which will now be discussed. First, a dynamic model of the MR shock strut is summarised. For a more detailed description, the reader is referred to Part 2. The landing impact model is then derived before a discussion the valve size optimisation methodology.

3.1 The MR shock strut model

A schematic diagram of the MR shock strut is shown in Figure 4. The design is based on the passive shock strut from the Institute of Aviation's I-23 aircraft, except where an MR valve is used in place of the conventional main orifice [10]. Figure 4 also presents the key equations used to formulate the shock strut model, which are described as follows.

Neglecting internal friction, the shock strut force F_s is readily derived using a pressure/area balance. The gas pressure is determined using the polytropic law for the compression of gases, where the key parameters are the gas exponent m, and the initial gas volume $v_{a0.}$ Fluid compressibility is modelled using the mass flow continuity equation, which introduces non-linear stiffness through the constant bulk modulus term β. Various investigators have used this form of hydraulic model to account for fluid compressibility in semi-active dampers [12-14]. However, previous work has not considered impact scenarios, where fluid compressibility effects will be particularly significant. Finally, the MR effect is characterised using the Buckingham equation for Bingham plastic flow between parallel flat plates [15]. In the dynamic model, this is formulated as a 3-D lookup table, which describes the MR valves quasi-steady pressure/flowrate performance as a function of yield stress [16]. The key

parameters in the Buckingham equation are the MR fluid viscosity μ, and the Bingham plastic yield stress τ_y, which can be determined from the MR fluid manufacturer's data.

As an aside, Patten, *et al*. [12] showed that the assumption of constant bulk modulus may not always be valid if there is a substantial change in pressure from the nominal value. Using the methods described by those authors, a variable bulk modulus term was also investigated but this yielded negligible performance differences with the more straightforward model. The constant bulk modulus assumption was therefore considered as valid in the present study.

3.2 The landing impact model

In this section, a two-degree-of-freedom (2DOF) landing impact model is derived. This is similar to that developed by Milwitzky and Cook [17] but summarised here for the sake of completeness. The model was designed to represent the Institute of Aviation's landing gear drop test rig without initial wheel rotation [10] i.e. wheel spin-up forces have been neglected.

A free-body diagram of the 2DOF impact model is shown in Figure 5. This corresponds to a telescopic type of landing gear, which is consistent with the experimental setup, where the relative displacement between the airframe and wheel assembly corresponds to the displacement of the shock. The equations of motion for the system are as follows:

$$\textit{Aircraft mass:}\quad m_p \ddot{z}_p = m_p g - L - F_s \tag{1}$$

$$\textit{Wheel mass:}\quad m_w \ddot{z}_w = m_w g - F_t + F_s \tag{2}$$

where m_p is the aircraft mass or drop mass, m_w is the mass of the wheel/tyre assembly**,** z_p and z_w are the displacements of the drop mass and wheel/tyre assembly respectively, L is the aerodynamic lift force from the wings, F_s is the shock strut force (see Figure 4) and F_t is the tyre force. The tyre force F_t was approximated using the following power law, which was shown by other investigators [17] to correlate well with observed behaviour:

$$F_t = cz_w^r \tag{3}$$

Here c and r are empirical constants. For simplification purposes, tyre hysteresis was neglected.

An added complexity in the model arises due to the initial shock strut inflation pressure P_{a0}, which generates an extension force. Assuming that the shock strut is rigid in compression and bending, the wheel and drop mass effectively remain locked until this initial force is overcome, i.e. the system behaves as a single-degree-of-freedom (SDOF) system [17]. Therefore two separate models are required with the SDOF model triggering the 2DOF model at the instant this initial force is exceeded. The equation of motion for the SDOF system is:

$$(m_p + m_w)\ddot{z} = (m_p + m_w) - L - F_t \tag{4}$$

where $z = z_p = z_w$. The initial condition for this SDOF model is set in terms of the sink velocity, V_{sink} $(= \dot{z}(0))$. At the instant $t = t_d$ when the shock strut begins to deflect, $F_s = P_{a0}a_{2o}$ (see Figure 4 and note that P_2=P_1). Substituting this expression into Eq.1 and noting from above that $\ddot{z}_p = \ddot{z}$ gives:

$$\ddot{z}_{t_d} = \frac{m_p g - L - P_{a0}a_{2o}}{m_p} \tag{5}$$

Eq.5 represents the critical acceleration to be exceeded to cause shock strut deflection and Eq.4 is solved until this value is reached. The 2DOF system is then triggered with the resulting initial conditions from the SDOF system at time $t = t_d$.

3.3 MR Valve geometry optimisation

The complete MR landing gear impact model has now been derived, and what remains is to determine the MR valve geometry. As some of the valve sizing work utilised existing and well known design techniques, only a summary will be provided in this text.

Rosenfeld and Wereley [18] developed a set of analytical rules to describe an optimal geometry of an MR valve. These rules, which are optimal in the sense that magnetic saturation is avoided as far as possible, were adopted in the present study. The method essentially involves defining three critical valve areas, and the geometry is generated so that they are equal. This helps maintain a constant flux density throughout the magnetic circuit so that a particular region does not prematurely saturate.

With reference to Figure 2(b), it can be shown that the resulting optimal geometry is completely defined by the following equations [18]:

$$t_a = 0.5\left(-(w_c + h) + \sqrt{0.5D^2 - (w_c + h)^2}\right) \tag{6a}$$

$$t_b = 0.5t_a \tag{6b}$$

where t_a is the bobbin core radius, D is the constrained MR valve diameter (which corresponds to a_{2i} in Figure 4), w_c is the coil width, h is the valve gap size and t_b is the bobbin flange height. With D being constant, Eq.6 is solved for a variety of coil widths w_c and for a constant valve gap h. The term w_c was calculated as the multiple of the coil diameter for 24-gauge copper wire (diameter = 0.516mm) with the number of coil wraps. Thus a '10 wrap' coil corresponds to a width of 10×0.516mm, and valve geometries were generated for wrap numbers between 4 and 16. The coil height h_c is dictated by the difference between the constrained total length l and the active valve length ($=2t_b$), and thus the number of coil turns

can be calculated. It is also useful to define a dimensionless valve length α, which is the fraction of the total length that is active (l_a/l). The optimal value is one.

Through inspection of Eq.6a, it can be observed how the bobbin core radius, and hence the active valve length (determined from Eq.6b), are independent of the total valve length. Thus for a fixed valve length, the packaging constraint on diameter may result in low dimensionless valve lengths, and hence performance could suffer. As shown in Figure 6, one method to overcome this constraint is to size a valve with a reduced length and then to stack identical valves together such that the total length remains unchanged. Devices with multiple stages have been investigated previously [19, 20], but to the authors' knowledge, investigators have not formally considered optimisation of the number of valve stages within a constrained space, which is the intention of the present study. The number of stages is defined in terms of a stage number n, and stage numbers between 1 and 4 were investigated.

So far, a methodology has been outlined to generate magnetically efficient valve geometries, but consideration has not yet been given to the valve's actual electrical and mechanical performance. Essentially, the MR valve should be able to achieve the maximum fluid yield stress without saturation of the magnetic circuit and without exceeding the maximum operating current of the solenoid wire. To assess the above requirements, an analytical methodology similar to that outlined in reference [21] was adopted. This proved to be relatively straightforward due to the equal critical areas of the valve. In summary, the method begins by defining the desired magnetic flux density in the fluid B_f (and hence magnetic field strength H_f) that is required to generate the maximum fluid yield stress. This was determined using the non-linear B-H curve for Fraunhofer AD57 MR fluid [22]. Next, the flux density in the valve material B_s was calculated using the principal of continuity of flux, and the corresponding field strength H_s was determined from the relevant B-H curve The valve

material was assumed to be 1018 mild steel due to its high magnetic permeability and good saturation properties. Nonetheless, the magnetic properties of this steel are still highly non-linear, and so it is important that B_s remains below the saturation level. Finally, the current I required to generate the magnetic field was determined using Kirchhoff's law. This should not exceed 2.5A, which was assumed as a reasonable maximum current for 24-gauge copper wire [18].

Some further important performance indicators that were calculated are as follows:

- The electrical power p required to generate maximum fluid yield stress.
- The time constant of the coil τ, which was calculated using the analogy of a resistance and inductance in series. A constant voltage source was assumed.
- The valve's control ratio λ, which is defined as:

$$\lambda = \frac{\Delta P_{\max}(Q_{\max}, \tau_{y_{\max}})}{\Delta P_0(Q_{mzx}, \tau_y = 0)} \quad (\lambda > 1) \tag{7}$$

where $\Delta P_{\max}$ is the maximum-field pressure drop and ΔP_0 is the zero field pressure drop. $\Delta P_{\max}$ was determined using the Buckingham equation (see Figure 4) as the summation of pressures across the active and inactive regions of the valve.

- The Reynolds number Re through the valve:

$$Re = \frac{\rho Q}{\mu b} \tag{8}$$

where ρ is the density of MR fluid (3290 kgm^{-3}), and b is mean annular circumference of the valve gap.

Some important points regarding the above analysis are as follows. The magnetic circuit analysis did not account for flux leakage into the fluid, which will slightly lower the flux density at the ends of the valve gap. However, this should not have a strong effect on the optimised geometry and performance, especially for a multiple-stage design.

The pressures calculated in Eq.7 are based on a quasi-steady flow model. The actual values will differ slightly from this due to fluid compressibility, which is the reason for developing the dynamic shock strut model.

Finally, the Reynolds number was considered important because the MR effect is strongly dependant on laminar flow, and previous research has suggested that turbulent flow regimes could reduce device performance [23]. For an MR landing gear, the onset of turbulence is more probable due to the associated higher velocities during impacts. The critical Reynolds number Re_c was approximated as the value for Newtonian flow between parallel flat plates. By using the hydraulic mean diameter and assuming a critical value of 2000 for pipe flow, this can be approximated as $Re_c = 1000$.

4 CASE STUDY

In what follows, the design methodology outlined in Section 2/Figure 3 is applied to a real aircraft using the numerical tools described in Section 4. Here, the aim is to size an MR landing gear for the Institute of Aviation's I-23 aircraft. With reference to Figure 3, the results in this section are organised as follows. First, the landing gear system is defined, along with the corresponding parameter values required by the numerical tools. Next, a preliminary design study is presented in order to calculate the desirable MR valve performance (ΔP_{max}, Q_{max}). This desirable performance is then used to calculate the 'optimal' valve size, which fully considers the constraints of the magnetic circuit. Finally, the impact

performance of the optimal design is investigated, where the aim is to demonstrate its potential to optimise damping for a wide range of input conditions.

4.1 System and parameter definitions

To begin the design process, experimental drop test data was obtained from a worst-case impact on the nose landing gear from the I-23 aircraft. Here, a drop mass corresponding to maximum payload, and the worst-case sink velocity was used. An equivalent MR model of this drop test was then developed using the numerical approach described in Sections 3.1 and 3.2.

Table 1 lists the parameters used to construct the equivalent model. For the MR shock strut model (see Figure 4), the parameters P_{a0}, v_{a0}, v_{10}, v_{20}, a_{2i}, and a_{2o} correspond to the actual I-23 nose gear values. The gas constant m was estimated as 1.1, which is a good approximation when the fluid and gas volumes are mixed [11]. With regards to the impact model, the parameters m_p, m_w, L, and V_{sink} correspond to the experimental drop test conditions. Furthermore, the tyre law constants c and r were determined by curve fitting to the compression phase of the tyre response from an impact test.

The final, and perhaps most important model parameters left to define, are the MR fluid's bulk modulus, yield stress, and viscosity. Referring to Table 1, the bulk modulus was approximated as 1.7GPa, which is the base value of a standard hydraulic oil [24]. This represents an ideal value but in practice, the MR fluid may contain entrained air, especially if mixing occurs between the fluid and gas volumes. In previous work by the authors [10], it was shown that the effect of a lower bulk modulus was to reduce the peak force and to increase the shock strut's deflection during an impact. Validation of the bulk modulus (which is dealt with in Part 2) will therefore be important. The viscosity was assumed as 0.1Pas, which corresponds to an extrapolated value taken from the fluid manufacturer's zero-field

viscosity/shear rate data at 25°C [22]. The maximum fluid yield stress $\tau_{y_{\max}}$ was estimated as 55kPa, which was measured at 25°C and at a shear rate of $1s^{-1}$ [22]. This is generated at a flux density of 0.7T with a magnetic field strength of 236kA/m.

4.2 Preliminary design

As shown in Figure 3, the first stage of the design process aims to determine a desirable valve performance (Steps 'A' to 'E'). This is achieved by calculating the MR valve geometry without a detailed consideration of the magnetic circuit. The total length *l* and diameter *D* of the MR valve are 45mm and 36mm respectively, which correspond to the geometrical constraints of the existing passive device. The mean valve diameter *d* and the dimensionless valve length α were chosen intuitively as 10mm and 0.5 respectively, giving an active valve length l_a equal to 22.5mm. The valve gap *h* is then determined using an iterative process by performing a worst-case landing impact simulation to achieve the desired performance at the maximum fluid yield stress of $\tau_{y_{\max}}$ = 55kPa.

Figure 7 presents the corresponding results, which shows the shock strut's force/time and force/displacement responses for a range of valve gap sizes. The worst-case experimental drop test data is also shown superimposed, which provides a useful performance benchmark. Clearly, *h* = 0.5mm results in large damping forces during the initial stage of the impact. For *h* = 0.65mm, damping levels are insufficient, and this results in large forces at the end of the impact due to excessive gas compression. The optimum response that provides the lowest peak force occurs when *h* = 0.57mm. Furthermore, it could be argued that this MR response is inherently superior to the passive system. For example, the fluctuation in force is less severe and maintains a more constant value throughout the impact. In other words, the MR response has a superior impact efficiency [11], which would provide an enhanced fatigue life

for the aircraft. This is a direct result of the Coulomb-viscous nature of the MR damping function, which provides large forces at low velocities. In contrast, the passive system has a quadratic damping function [17], which results in larger fluctuations in the overall shock strut force.

Referring to the design flowchart (Figure 3), the desirable valve performance was then determined as ΔP_{max} = 12.2MPa, which occurred at $Q_{max} = 2\times10^{-3}$ m^3s^{-1} during the optimum impact response (h = 0.57mm).

4.3 Optimal design

The preliminary design can now be optimised by considering magnetic circuit issues as well as the pressure/flow requirements. This corresponds to steps 'F' to 'I' in Figure 3. The key aims are as follows:

- To achieve the desired valve performance (ΔP_{max}, Q_{max}) at maximum yield stress
- To achieve the maximum yield stress without saturation of the steel, and without exceeding the maximum current rating of the copper wire.
- To maximise the control ratio, and hence the range of impacts that can be optimally damped.

Figure 8 presents the performance results of each valve for wrap numbers between 4-16 and for stage numbers equal to 1 and 3. Where applicable, the results were calculated with the maximum flow rate from the preliminary design ($Q_{max} = 2\times10^{-3}$ m^3s^{-1}), and at the maximum yield stress $\tau_{y_{max}}$ = 55kPa. Furthermore, the results are shown for two valve gap sizes - the preliminary valve gap size (h = 0.57mm), and h = 0.59mm, which transpires to be the optimal design, as will be illustrated in the following analysis.

First, Figure 8(a) plots the magnetic flux density that will result in the steel in order to generate maximum yield stress in the fluid. This is shown as a function of wrap number and since the critical valve area is independent of the total valve length, the results are independent of the stage number. The saturation limit of the steel (1.3T) is exceeded for valve geometries with a wrap number greater than 12. These geometries were therefore eliminated from the design process. Also, it is important to note how the magnetic flux density is independent of the valve gap size.

Figure 8(b) shows the control ratio for each valve configuration. This result illustrates the key advantage of stacking geometrically similar valves together, since superior performance is achieved with increasing stage number. The effect of the valve gap size h on the control ratio is fairly significant.

The above results suggest that the optimum valve design must have a low wrap number and a high stage number. However, they fail to recognise the implications that such valve configurations have on the required current, which is now addressed in Figure 8(c). Lower currents are associated with an increasing wrap number and a decreasing stage number. As stated earlier, 2.5A was considered as the maximum safe operating current for the copper wire and this eliminated a 4-stage valve design (not shown in Figure 8(c)). The 3-stage-12-wrap design appears to provide the optimal configuration where superior control ratios are achieved with acceptable current levels. Furthermore, note how the valve gap size has no significant impact on the required current, and hence the optimal wrap and stage number.

A further advantage of a multi-valve configuration is a reduced time constant, which is observed in Figure 8(d) for increasing stage number and decreasing wrap number. Again, as with the previous performance indicators (except control ratio), the time constant is largely independent of the valve gap size.

Next, the Reynolds number (which is independent of stage number) is investigated in Figure 8(e). Clearly, the Reynolds number remains below the critical value at the maximum anticipated flow rate during the impact. This is a promising result and suggests that valve performance should not be inhibited by turbulent flow. Also, the valve gap size has a negligible influence on performance.

Using the above results, it can be deduced that a 3-stage-12-wrap valve provides the optimal configuration. However, obtaining the desired maximum field performance (ΔP_{max} = 12.2MPa) has been neglected, which is now addressed in Figure 8(f). As illustrated in the above results, the valve gap size h has no significant effect on the optimum wrap and stage number. Therefore, it is straightforward to tune h as a final step in order to achieve the desired pressure drop. This is shown in Figure 8(f), where it can be observed that the optimum 3-stage-12-wrap valve correlates well with the desired performance when h is equal to 0.59mm.

The key geometrical parameters and performance indicators of the optimal 3-stage-12-wrap valve design are given in Table 2. In summary, this design maximises the dimensionless valve length (α = 59%) and hence control ratio (λ = 2.26), without magnetic saturation (B_s < 1.3T), and without significantly exceeding the 2.5A rating of the copper wire. For example, the maximum yield stress is achieved at 2.6A, which could be sustained for short periods of time. Furthermore, this was found to require just 16.5W of power, and could be supplied by a low voltage source of 2.1V, or 6.3V, depending on whether the individual stages are wound in parallel or series. Also, the optimal design has a time constant of 19ms. In practice, if a current driver is used (the definition of time constant assumed constant voltage) and the coils are arranged in parallel, the time constant will be lower than this value [25].

To further clarify the performance of this optimised geometry, Figure 9 compares its quasi-steady pressure-flowrate characteristic with the preliminary valve design. Clearly, excellent correlation is observed, which suggests that the desired impact performance will be achieved. Furthermore, it can be observed that the optimal valve has a slightly superior control ratio. This is a result of the conservative estimate of dimensionless valve length (α = 50%) that was assumed in the preliminary sizing analysis.

4.4 MR landing gear impact performance

In this section, the optimal valve geometry is investigated within the aircraft landing gear impact simulation. It is assumed that the full range of fluid yield stress can be generated, which is a valid assumption after consideration of the results in the previous section.

First, Figure 10 presents the worst-case landing impact results, which is compared to the experimental (passive) data, and to the preliminary valve's performance. As shown, the desired performance is still maintained, and no further refinements to the valve design are necessary. This demonstrates the robustness of the proposed design methodology.

Next, to illustrate the controllability of the optimised design, Figure 11 presents the impact responses of the shock strut with less severe input conditions. The results are shown in open-loop control i.e. where the yield stress is maintained constant throughout the impact. Device control is outside the scope of the present study. Nonetheless, this serves as a useful example, and illustrates the potential to optimise impact performance for a wide range of disturbance conditions.

In Figure 11, results for two different input excitations are shown. The 'soft impact' uses the original drop mass (see Table 1), but lowers the sink velocity to the minimum anticipated

value: V_{sink} = 1m/s. The 'very soft impact' also has a sink velocity of 1m/s, but simulates a drop mass of just 284kg, which is 60% of the original (maximum) value.

For the soft impact, it can be observed that lowering the yield stress from 55kPa (the maximum value) to 6kPa, best minimises the force during the impact. Furthermore, the maximum yield stress response is a good indicator of the wide range of controllable force that is available. As before, the MR impact response is inherently efficient without using closed-loop control.

For the very soft impact, the control limits of the design can be observed. For example, it could be argued that the damping provided by the base viscosity of the fluid (τ_y = 0kPa), results in damping forces that are slightly high during the initial stages of the impact. This is best observed in Figure 11(b), where it can be observed that the forces at the end of the impact are lower. Nonetheless, the impact efficiency is still good.

5 CONCLUSIONS

In this paper, a sizing methodology was developed for MR landing gear shock struts. Using packaging requirements as a key constraint, the aim was to maximise the device's control ratio and to optimise the magnetic design. Consequently, the semi-active landing gear can produce desirable behaviour for a wide range of impact conditions, unlike a passive device.

A 2DOF landing impact model and valve size optimisation techniques were used to implement the design methodology. The impact model was designed to be equivalent to an existing landing gear drop test facility, which permitted accurate design assessments. Furthermore, the model accounted for fluid compressibility which is important when considering device control, especially under impulsive loading. To maximise device

controllability, it was shown how to optimise the valve's stage number within a constrained space.

The impact model used a fluid mechanics based approach which has been previously proposed in the literature. However, to the authors knowledge, the previous work has not considered impact scenarios, or the packaging/design constraints that are applicable to landing gears.

In order to illustrate the proposed design methodology, a case study was presented that sized an MR valve for the nose gear of an I-23 aircraft. The methodology proved to be very robust, where the desired worst-case impact performance of the magnetically optimised valve was accurately achieved. Moreover, a widely adjustable valve control ratio resulted in damping levels that could accommodate a large range of impact conditions. Therefore, when combined with an appropriate control strategy, the optimised design should demonstrate significant advantages over a passive system. Even in open-loop control (i.e. constant yield stress), it was shown how the MR effect provides inherently superior damping performance over a conventional passive orifice. For example, the impact efficiency, and hence the severity of fatigue loading is much improved.

The present paper makes an important first step to help demonstrate the feasibility of an MR landing gear. However, the results were based on a time-domain model that has assumed values for certain parameters. Consequently, the model needs validating, and this will be addressed in Part 2 of this contribution.

Feasibility will also be dependant on fail-safety, which was not directly considered in this study i.e. in the event of a power failure, and the subsequent loss of the MR effect, the landing gear must provide acceptable damping performance during a worst-case landing. A novel

solution might incorporate a permanent magnet within the MR valve [26], which could be designed by updating the numerical sizing tools presented in this paper.

6 REFERENCES

1. Krüger, W (2002), "Design and simulation of semi-active landing gears for transport aircraft", *Mechanics of Structures and Machines*, **30**(4), 493-526.
2. McGehee, J R and Carden, H D (1976), "A mathematical model of an active control landing gear for load control during impact and roll-out", *NASA Technical Note*, **NASA TN D-8080**.
3. Brookes, D A (1982), "Electro-Rheological Devices", *Chartered Mechanical Engineer*, September, pp 91-93.
4. Sims, N D, Stanway, R, and Johnson, A R (1999), "Vibration control using smart fluids: A state-of-the-art review", *The Shock and Vibration digest*, **31**(3), 195-203.
5. Ma, Y, Zhang, Y, and Lu, K (1998), "Frequency and temperature dependence of complex stronium titanate electrorheological fluids under an alternating electric field", *Journal of Applied Physics*, **83**, 5522-5524.
6. Carlson, J D, Catanzarite, D M, and St. Clair, K A (1996), "Commercial magnetorheological fluid devices", *Proceedings of the 5th International Conference on Electrorheological Fluids, Magnetorheological Suspensions and Associated Technology*: World Scientific Publishing, Singapore.
7. Lou, Z, Ervin, R D, Filisko, F E, and Winkler, C B (1993), "Electrorheologically controlled landing gear", *Aerospace Engineering (Warrendale, Pennsylvania)*, **13**(6), 17-22.
8. Berg, C D and Wellstead, P E (1998), "The application of a smart landing gear oleo incorporating electrorheological fluid", *Journal of Intelligent Material Systems and Structures*, **9**(8), 592-600.
9. Choi, Y T and Wereley, N M (2003), "Vibration control of a landing gear system featuring electrorheological/magnetorheological fluids", *Journal of Aircraft*, **40**(3), 432-439.
10. Batterbee, D C, Sims, N D, Stanway, R, and Wolejsza, Z (2005), "Design and performance optimisation of magnetorheological oleopneumatic landing gear", *SPIE Annual International Symposium on Smart Structures and materials: Damping and Isolation*, **5760-10**.
11. Currey, N S (1988), *"Aircraft Landing Gear Design: Principles and Practices"*, American Institute of Aeronautics and Astronautics, Inc.
12. Patten, W N, Mo, C, Kuehn, J, and Lee, J (1998), "A primer on design of semiactive vibration absorbers (SAVA)", *Journal of Engineering Mechanics - ASCE*, **124**(1), 61-68.
13. Symans, M D and Constantinou, M C (1997), "Experimental testing and analytical modeling of semi-active fluid dampers for seismic protection", *Journal of Intelligent Material Systems and Structures*, **8**, 644-657.
14. Wang, X and Gordaninejad, F (2001), "Dynamic Modelling of Semi-Active ER/MR Fluid Dampers", *Damping and Isolation, Proceedings of SPIE Conference on Smart Materials and Structures*, **4331**.

15. Peel, D J and Bullough, W A (1994), "Prediction of ER valve performance in steady flow", *Proceedings of the Institution of Mechanical Engineers, Part C: Journal of Mechanical Engineering Science*, **208**, 253-266.
16. Sims, N D, *et al.* (2000), "The electrorheological long-stroke damper: A new modelling technique with experimental validation", *Journal of Sound and Vibration*, **229**(2), 207-227.
17. Milwitzky, B and Cook, F E (1952), "Analysis of landing-gear behavior", *NACA Report*, **1154**.
18. Rosenfeld, N C and Wereley, N M (2004), "Volume constrained optimization of magnetorheological and electrorheological valves and dampers", *Smart Materials and Structures*, **13**, 1303-1313.
19. Sodeyama, H, *et al.* (2003), "Dynamic tests and simulation of magneto-rheological dampers", *Computer-Aided Civil and Infrastructure Engineering*, **18**(1), 45-57.
20. Yang, G, Spencer Jr., B F, Jung, H-J, and Carlson, J D (2004), "Dynamic modeling of large-scale magnetorheological damper systems for civil engineering applications", *Journal of Engineering Mechanics*, **130**(9), 1107-1114.
21. Lord MR Solutions (1999), "Magnetic circuit design", *Engineering note*, http://www.lord.com/Portals/0/MR/Magnetic_Circuit_Design.pdf.
22. Fraunhofer Institut Silicatforschung (2005), http://www.isc.fraunhofer.de/.
23. Ahmadian, M and Norris, J A (2004), "Rheological controllability of double-ended MR dampers subjected to impact loading", *SPIE Annual International Symposium on Smart Structures and Materials: Damping and Isolation*, **5386-20**.
24. Stringer, J D (1976), *"Hydraulic Systems Analysis"*, The Macmillan Press Ltd.
25. Yang, G, Spencer Jr, B F, Carlson, J D, and Sain, M K (2002), "Large-scale MR fluid dampers: Modelling and dynamic performance considerations", *Engineering Structures*, **24**, 309-323.
26. Carlson, J D (2002), "Permanent-electromagnet systems ("magnetic cancellation")", *Lord Corporation Engineering Note*, http://literature.lord.com/root/other/rheonetic/Permanent_Electromagnet_Systems.pdf.

ACKNOWLEDGEMENTS

The authors are grateful for the support of the European Commission under project reference No. FP6-502793 (The ADLAND project). The authors would also like to acknowledge the EPSRC for the studentship awarded to D.Batterbee.

	Parameter	Symbol/unit	Value
MR Shock strut	Initial gas pressure	P_{a0} /bar	9.5
	Initial gas volume	v_{a0} /cm^3	170
	Initial fluid volume of chamber 1	v_{10} /cm^3	201
	Initial fluid volume of chamber 2	v_{20} /cm^3	132
	Inner area of the inner cylinder	a_{2i}/cm^2	10.18
	Outer area of the inner cylinder	a_{2o}/cm^2	13.85
	Gas constant	m/-	1.1
Impact	Drop mass	m_p/kg	473
	Mass of wheel/tyre assembly	m_w/kg	4.7
	Lift force	L/N	3120
	Sink velocity	V_{sink}/ ms^{-1}	2.43
	Tyre constant	c/-	8×10^6
	Tyre exponent	r/-	2.26
Fluid	Maximum yield stress	$\tau_{y_{\max}}$ /kPa	55
	Flux density at $\tau_{y_{\max}}$	B_f/T	0.7
	Magnetic field strength at $\tau_{y_{\max}}$	H_f/kAm^{-1}	236
	Bulk modulus	β /GPa	1.7
	Viscosity	μ /Pas	0.1

Table 1: MR landing impact model parameters

	Parameter	Symbol/unit	Value
Geometry	Length of 1 valve	l /mm	15
	Stage number	n/-	3
	Wrap number	-	12
	Valve gap height	h /mm	0.59
	Bobbin core radius	t_a /mm	8.88
	Flange height	t_b /mm	4.44
	Mean valve diameter	d /mm	30.72
	Valve diameter	D /mm	36
	Number of turns of gauge-24 wire	N/-	132
Performance	Dimensionless valve length	α/-	0.59
	Flux density in the steel at maximum yield stress	B_S /T	1.2
	Current to achieve $\tau_{y_{\max}}$	I /A	2.6
	Power to achieve $\tau_{y_{\max}}$	P/W	16.5
	Maximum pressure drop at $\tau_{y_{\max}}$	ΔP_{max} /MPa	12.3
	Control ratio (at $Q_{max} = 2\times10^{-3}$ m^{3}s^{-1})	λ/-	2.26
	Reynolds number (at $Q_{max} = 2\times10^{-3}$ m^{3}s^{-1})	Re/-	680
	Time constant	τ /ms	19

Table 2: Geometry and key performance indicators of the optimised valve

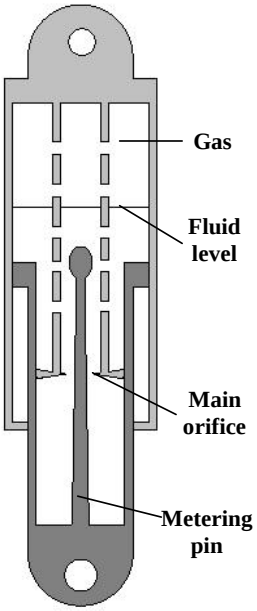

Figure 1: Schematic representation of a passive oleopneumatic shock absorber.

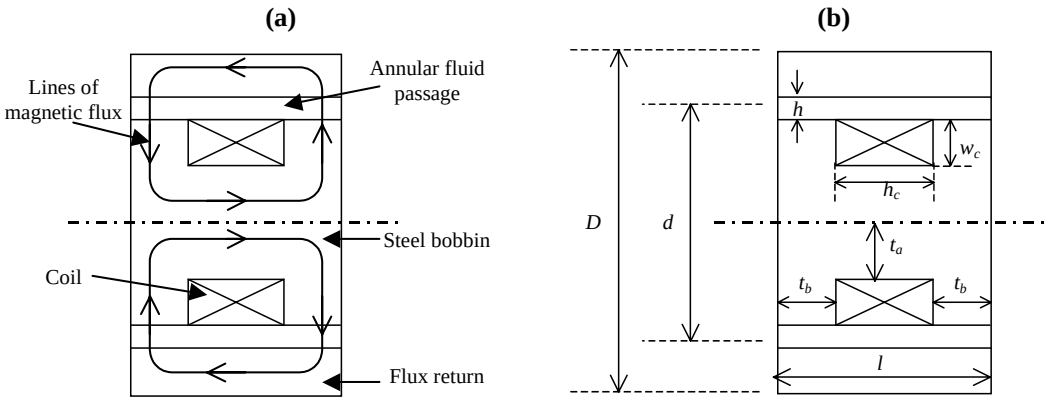

Figure 2: A flow mode MR valve. (a) Valve configuration and (b) valve nomenclature.

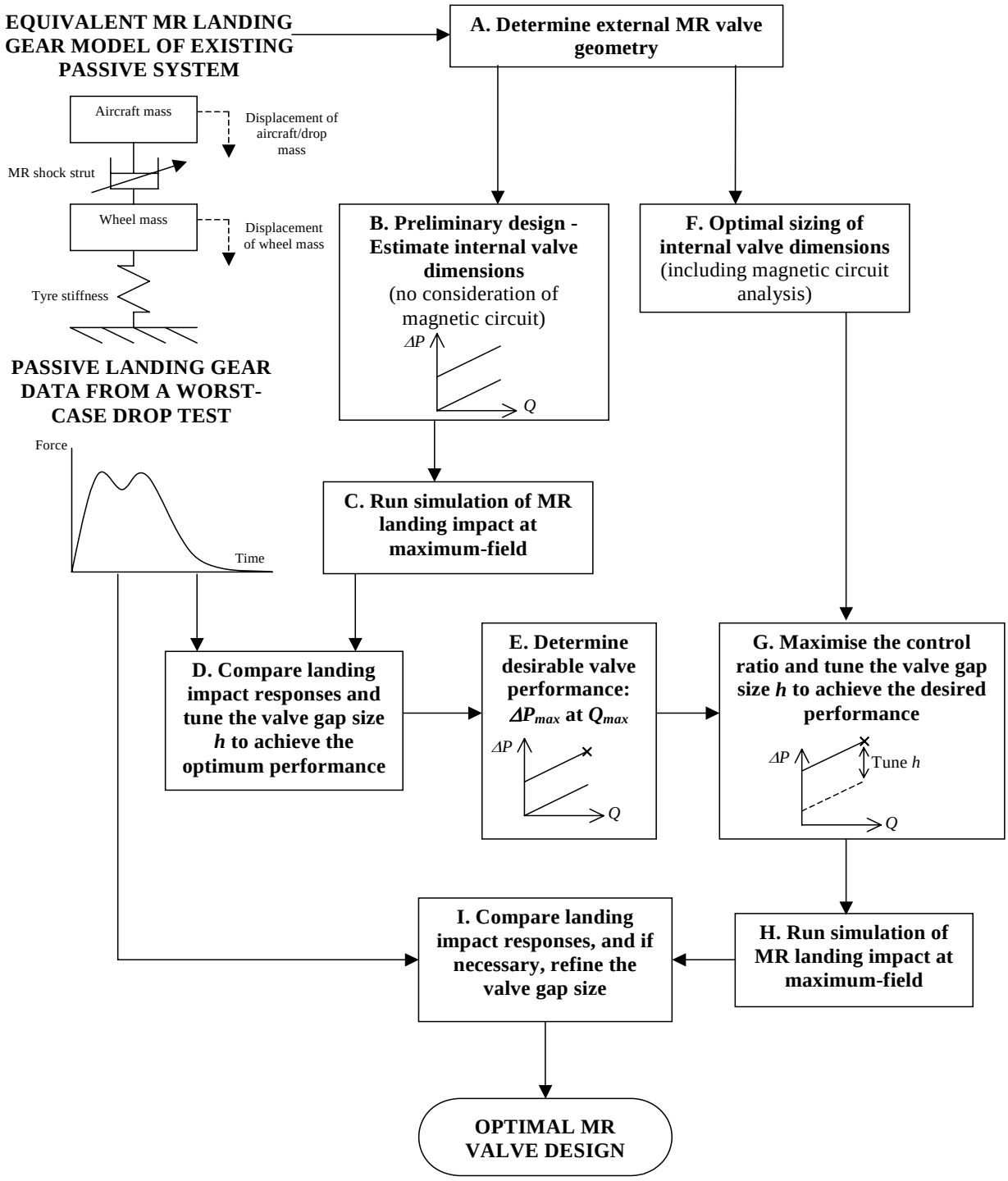

Figure 3: A flowchart describing the design methodology

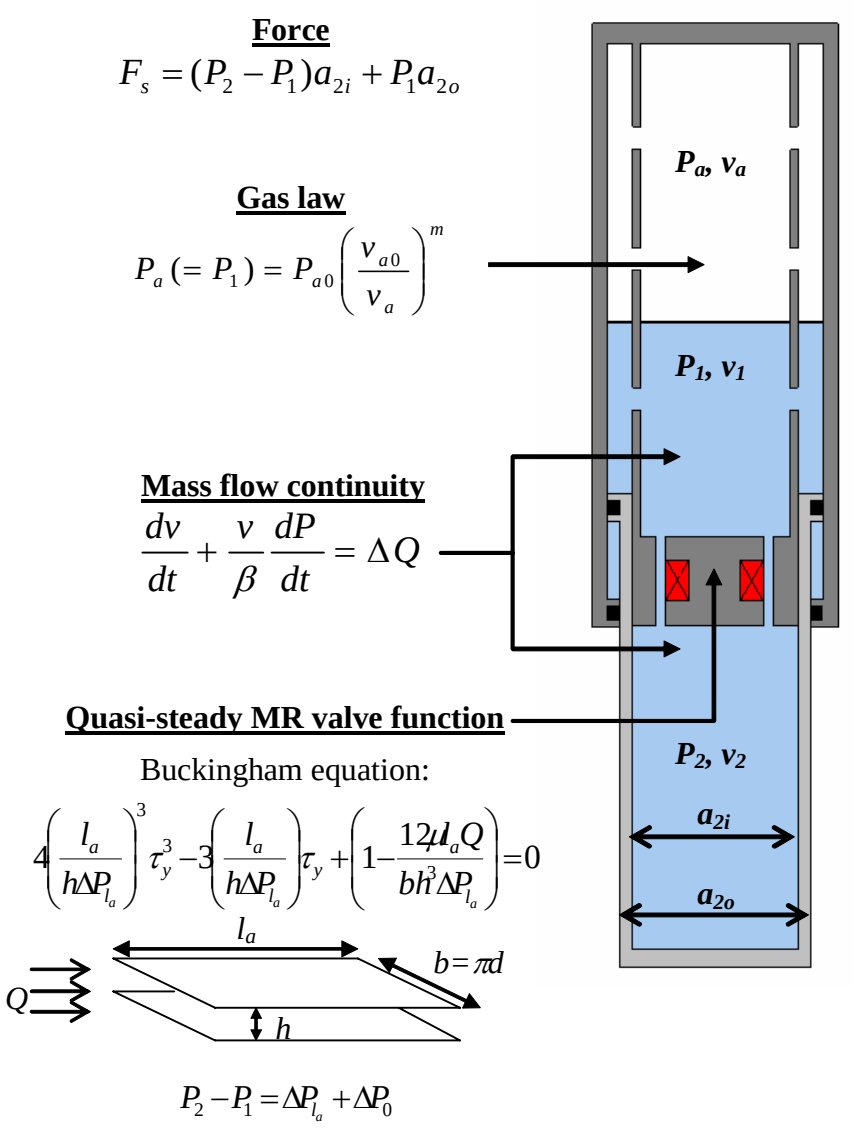

Figure 4: Summary of the dynamic MR shock strut model.

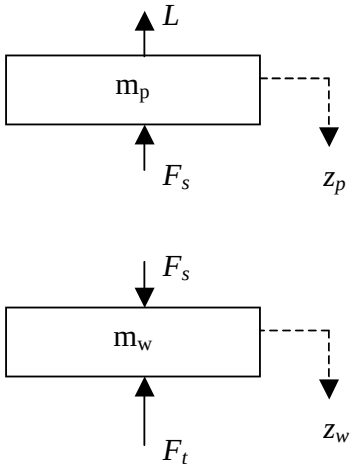

Figure 5: Free-body diagram of the landing impact model.

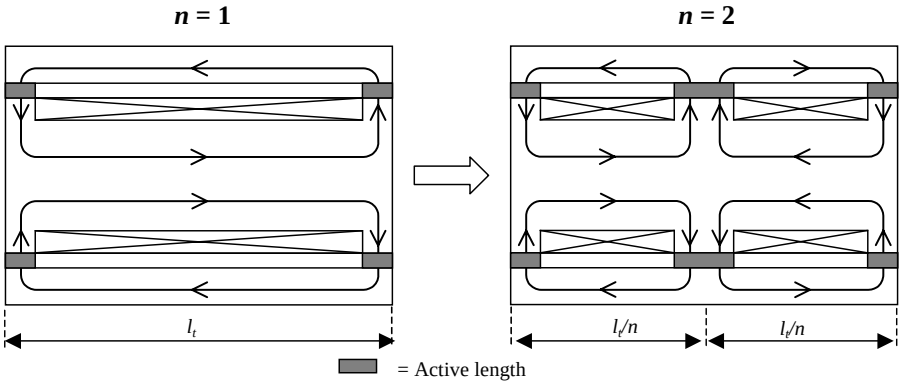

Figure 6: Improving dimensionless valve length using the stacking method.

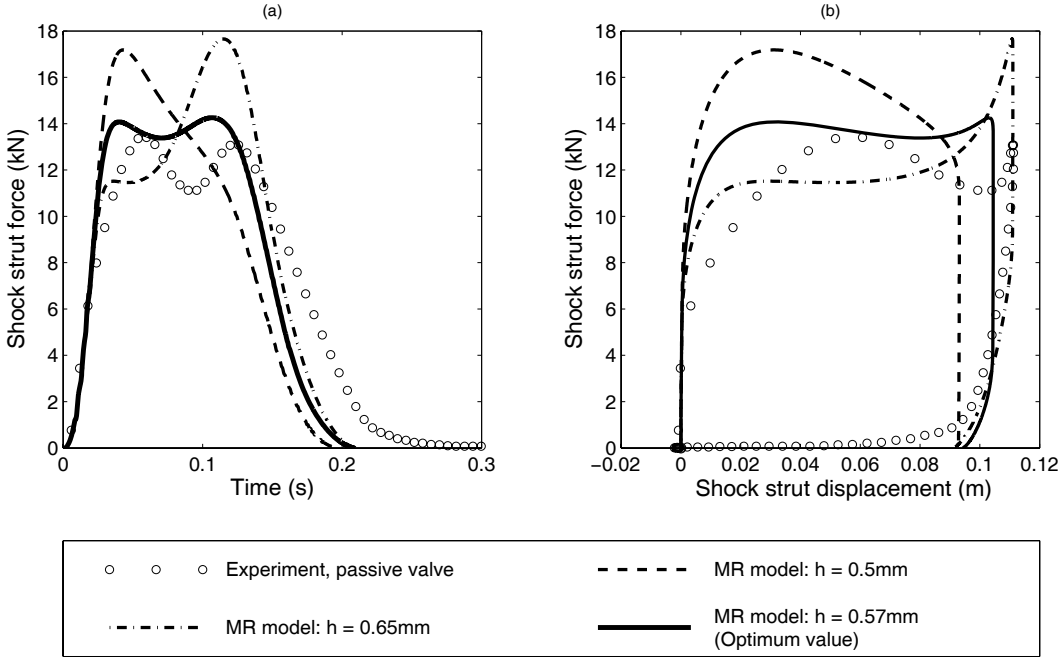

Figure 7: Tuning the valve gap size to achieve the desired worst-case landing impact performance. τ_y = 55kPa.

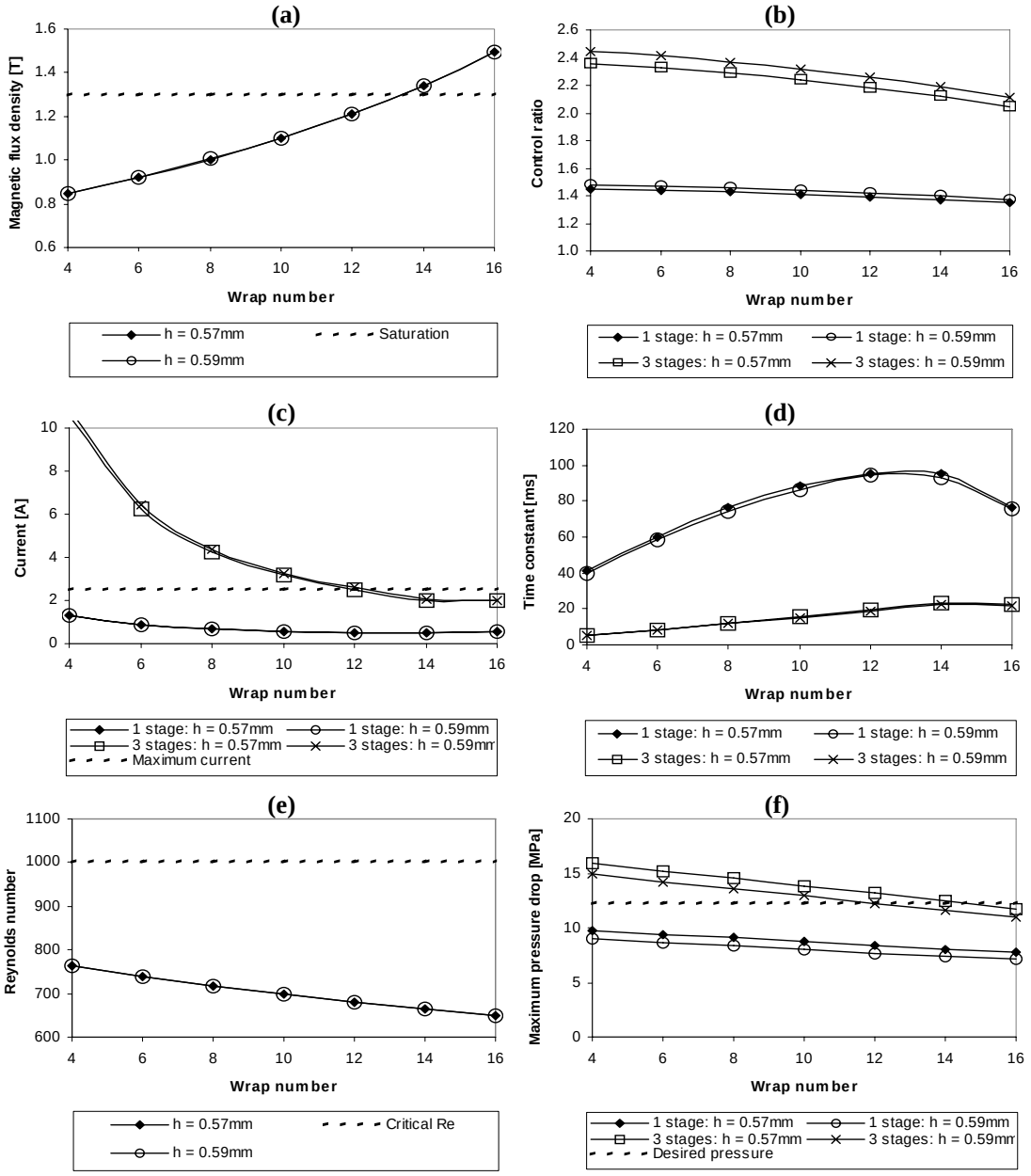

Figure 8: MR valve sizing results. (a) Magnetic flux density, (b) control ratio, (c) current, (d) time constant, (e) Reynolds number, and (f) maximum pressure drop. $Q = 2\times10^{-3}$ m^{3}s^{-1}, $\tau_y = 55$kPa.

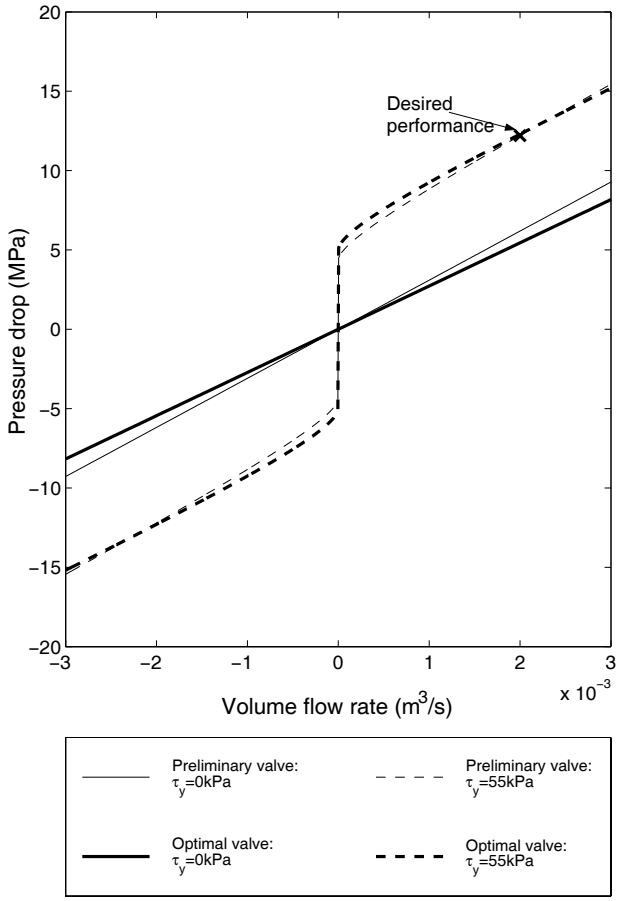

Figure 9: Pressure/flowrate characteristics comparing the preliminary and optimal valve designs.

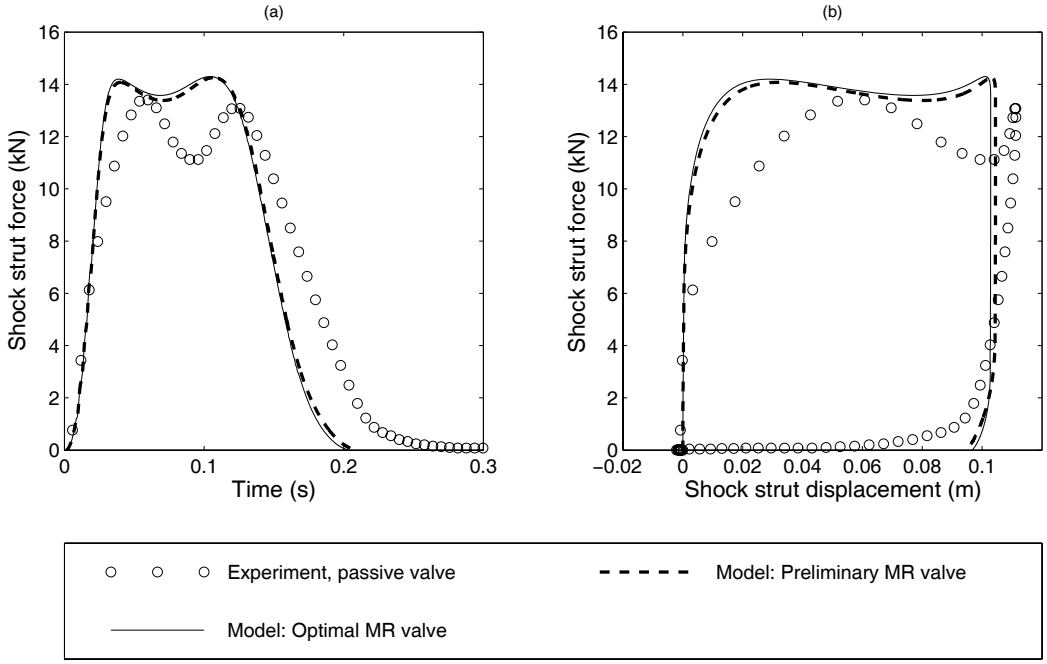

Figure 10: Worst case landing gear impact performance with the optimal geometry. τ_y = 55kPa.

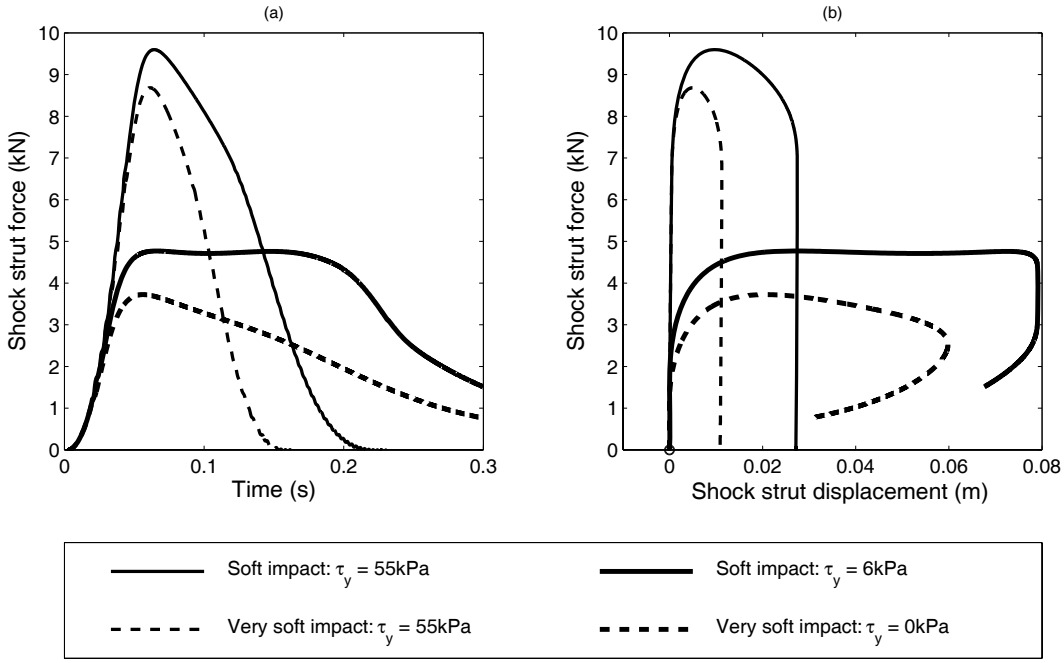

Figure 11: Landing gear impact performances with less severe input conditions. Soft impact: m_p = 473kg and V_{sink} = 1m/s. Very soft impact: m_p = 284kg and V_{sink} = 1m/s.